The Journal of Chemical Physics

RESEARCH ARTICLE | JUNE 20 2023

Photoelectron spectroscopy from a liquid flatjet

Dominik Stemer ; Tillmann Buttersack ; Henrik Haak ; Sebastian Malerz ; Hanns Christian Schewe ; Florian Trinter ; Karen Mudryk ; Michele Pugini ; Bruno Credidio ; Robert Seidel ; Uwe Hergenhahn ; Gerard Meijer ; Stephan Thürmer ; Bernd Winter

J. Chem. Phys. 158, 234202 (2023)
https://doi.org/10.1063/5.0155182

The Journal of Chemical Physics ARTICLE scitation.org/journal/jcp

Photoelectron spectroscopy from a liquid flatjet

Cite as: J. Chem. Phys. 158, 234202 (2023); doi: 10.1063/5.0155182
Submitted: 18 April 2023 • Accepted: 26 May 2023 •
Published Online: 20 June 2023

Dominik Stemer,[1,a)] Tillmann Buttersack,[1] Henrik Haak,[1] Sebastian Malerz,[1] Hanns Christian Schewe,[2] Florian Trinter,[1,3] Karen Mudryk,[1] Michele Pugini,[1] Bruno Credidio,[1] Robert Seidel,[4] Uwe Hergenhahn,[1] Gerard Meijer,[1] Stephan Thürmer,[5] and Bernd Winter[1]

AFFILIATIONS

[1] Fritz-Haber-Institut der Max-Planck-Gesellschaft, Faradayweg 4-6, 14195 Berlin, Germany
[2] Institute of Organic Chemistry and Biochemistry, Czech Academy of Sciences, Flemingovo nám. 2, 16610 Prague 6, Czech Republic
[3] Institut für Kernphysik, Goethe-Universität Frankfurt, Max-von-Laue-Str. 1, 60438 Frankfurt am Main, Germany
[4] Helmholtz-Zentrum Berlin für Materialien und Energie, Hahn-Meitner-Platz 1, 14109 Berlin, Germany
[5] Department of Chemistry, Graduate School of Science, Kyoto University, Kitashirakawa-Oiwakecho, Sakyo-Ku, 606-8502 Kyoto, Japan

[a)] **Author to whom correspondence should be addressed:** dstemer@fhi-berlin.mpg.de

ABSTRACT

We demonstrate liquid-jet photoelectron spectroscopy from a flatjet formed by the impingement of two micron-sized cylindrical jets of different aqueous solutions. Flatjets provide flexible experimental templates enabling unique liquid-phase experiments that would not be possible using single cylindrical liquid jets. One such possibility is to generate two co-flowing liquid-jet sheets with a common interface in vacuum, with each surface facing the vacuum being representative of one of the solutions, allowing face-sensitive detection by photoelectron spectroscopy. The impingement of two cylindrical jets also enables the application of different bias potentials to each jet with the principal possibility to generate a potential gradient between the two solution phases. This is shown for the case of a flatjet composed of a sodium iodide aqueous solution and neat liquid water. The implications of asymmetric biasing for flatjet photoelectron spectroscopy are discussed. The first photoemission spectra for a sandwich-type flatjet comprised of a water layer encapsulated by two outer layers of an organic solvent (toluene) are also shown.

I. INTRODUCTION

The development of liquid-jet photoelectron spectroscopy (LJ-PES) about 30 years ago made it possible to study the ground- and excited-state electronic structure of liquid water, as well as aqueous and organic solutions, with chemical-state specificity[1–5] — including electronic decay pathways,[6,7] nuclear dynamics,[8] and interfacial interactions.[9–12] Valence and core-level LJ-PES have been reviewed several times over the past 15 years.[13–15]

With a single exception,[16] previous LJ-PES studies have exclusively utilized cylindrical liquid jets (LJs) of typically 10–50 μm in diameter, which are injected into vacuum through a suitable nozzle. In contrast to cylindrical jets, liquid flatjets (FJs) have recently begun to attract considerable attention due to their thin and nearly planar target geometry, which promises to enable many unique experiments. FJs are typically generated by the impingement of two cylindrical jets (the most common approach),[17–20] by the injection of a single solution through a slit-shaped orifice,[21–24] or by the compression of a cylindrical jet by a transverse gas flow.[25]

Among the most salient advantages of a FJ over a cylindrical LJ is the possibility to generate extremely thin liquid-phase targets. As mentioned, LJs tend to have thicknesses of 10–50 μm, while FJs may be readily generated with thicknesses ranging from 50 nm to 5 μm, depending on the approach used and the position on the FJ probed.[21,24,25] Extremely thin liquid targets enable a wide range of previously inaccessible liquid-phase experiments based on transmission spectroscopy, including X-ray absorption spectroscopy (XAS) of neat liquid water and aqueous solutions.[19,23,25,26] With

cylindrical jets, such absorption-based experiments were generally only possible below (within the so-called water window) or far above (hard X-rays) the O 1s core-level absorption edge due to the intense absorption of light over the relatively long liquid-phase path length.

In addition to tunable thickness, the flat surface of the FJ is a crucial advantage for experiments requiring a well-defined planar geometry, for example, molecular-beam scattering off of a liquid target.[27] Another exciting possibility is the potential to measure photoelectron angular distributions (PADs) for oriented molecules at the liquid–vapor interface. The curved sample geometry of a typical LJ is a critical drawback in this context, due to the averaged take-off angle, with respect to the surface normal, of the photoelectrons upon photoionization. Indeed, despite the preference of water molecules at the liquid–vapor interface to orient with their dipole axis close to the interfacial plane,[28,29] previous PAD studies of liquid water using cylindrical jets have not observed orientational effects.[30,31] A flat surface, which can also be freely oriented with respect to the light and detection directions, would constitute a more appropriate sample for studies focused on characterizing the presence and degree of molecular orientation at the interface. It should be noted, however, that the higher gas pressure associated with evaporation from the planar surface of FJs may complicate experiments due to a larger prominence of undesired scattering of electrons with (water) vapor, which would tend to smear out an original angular distribution.[30–32]

Beyond serving as a convenient platform to measure orientation-induced effects, a FJ may also be useful for inducing the orientation of molecules at the liquid–vapor or liquid–liquid interface through the application of an asymmetric bias potential, with potential implications for controlling interfacial reaction kinetics. Such an orientation of water molecules may be readily achieved at the liquid–solid interface through the application of a suitable electric potential to the solid surface, as has been confirmed by a variety of experimental approaches, including X-ray scattering,[33] surface-enhanced infrared absorption spectroscopy,[34] and vibrational sum-frequency spectroscopy.[35,36] A recent study suggests that similar effects may also occur at the liquid–vapor interface,[37] indicating that induced orientation may be achievable in a FJ system as well, if a suitable voltage gradient could be generated across the first FJ leaf.

FJs take the form of a thin fluid sheet, followed by a succession of mutually orthogonal links, each composed of a thin leaf-shaped sheet bounded by relatively thick fluid rims. This shape results from the combined influence of surface tension and fluid inertia (see Fig. 1). The dimensions of the leaves depend on multiple parameters, including fluid viscosity, flow rate, impinging angle, and jet-nozzle diameter.[18] In the specific case where a FJ is generated from the impingement of two cylindrical microjets of different solutions, our recent study based on chemiluminescence from two reacting solutions revealed that, under laminar flow conditions, the first generated leaf is composed of two distinct co-flowing liquid sheets that share a liquid–liquid interface. This interface only blurs slightly along the flow direction as a result of solution interdiffusion.[20] This sort of mixed FJ constitutes a unique and flexible experimental template for X-ray studies of liquid–liquid interfaces, as well as for the reactions that take place there, as different positions along the reaction coordinate may be accessed simply by focusing on different spatial coordinates along the FJ's downstream coordinate. This system is also exceptionally suitable for the study of reactions with fast kinetics, enabling the probing of reacting species as soon as they come into contact and of products immediately upon formation.[20,38] Due to the buried nature of the liquid–liquid interface, we anticipate that X-ray emission spectroscopy (XES), X-ray absorption spectroscopy (XAS), and nonlinear optical spectroscopy will greatly complement PES studies of mixed FJs.

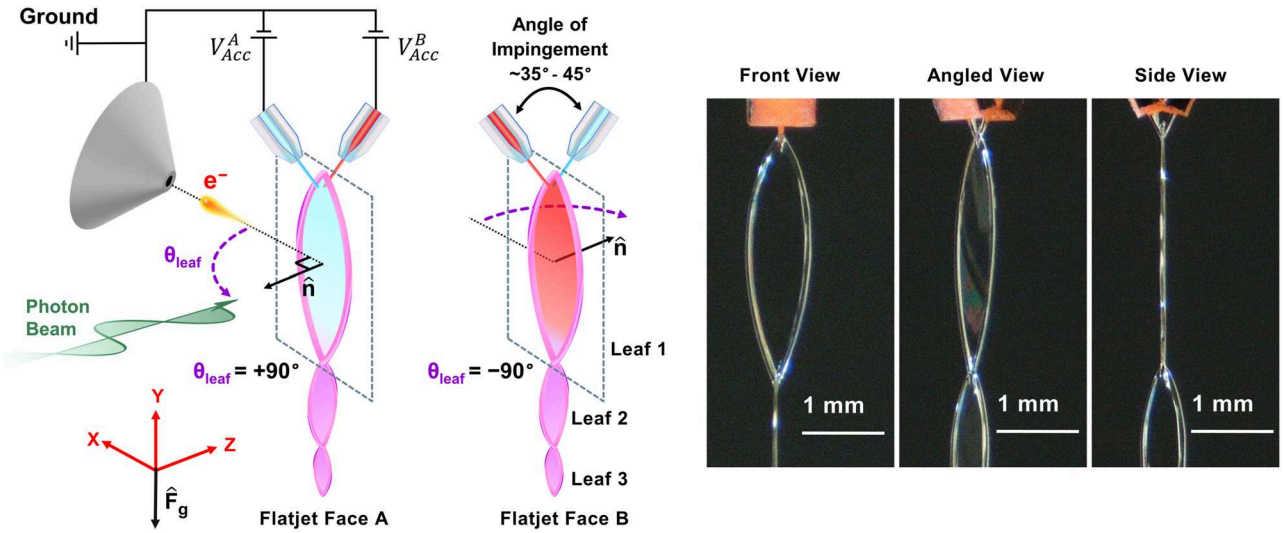

FIG. 1. Experimental schematic for photoelectron spectroscopy (PES) measurements from a liquid flatjet (FJ, left) with photographs of our FJ in operation (right). The FJ is formed via the impingement of two cylindrical jets and provides a sufficiently large surface for PES measurements. The FJ may be rotated about the downstream propagation axis (here the y-axis) around the angle θ_{leaf} using a suitable manipulator such that both faces of each leaf may be probed. We define $\theta_{leaf} = 0°$ such that the surface of the first leaf is perpendicular to the detector axis (the x-axis), here exemplified by the orifice of the detector (electron skimmer). The electric connections enabling the application of accelerating bias voltages V^A_{Acc} and V^B_{Acc} to each cylindrical jet are sketched at the top left.

Here, we apply flatjet photoelectron spectroscopy (FJ-PES) to study the two faces of a mixed FJ generated by the impingement of dissimilar aqueous solutions and organic liquids. Driven by our recent work on the determination of accurate and absolute electron energetics from aqueous solutions, as measured from electrically biased cylindrical LJs, we utilize PES as a sensitive probe of effective (real) surface potentials.[39,40] We also exploit the fact that different bias voltages can be applied to the two cylindrical jets prior to impingement. We explore the possibilities of this new asymmetric biasing scheme, with implications for the generation of an electric-potential gradient across the thickness of the FJ leaf itself. Finally, we investigate a unique sandwich-style FJ comprised of a central water sheet fully encapsulated by two outer sheets of an organic liquid.

II. METHODS

We developed a custom impingement-based FJ system involving the use of two independent cylindrical liquid microjets, each driven by their own high-performance liquid-chromatography (HPLC) pump (Shimadzu LC-20AD). We injected the two solutions into vacuum through either PEEK tubing or quartz capillaries with equal inner diameters of 64 μm at an impingement angle of 35°–45°. This approach enabled us to generate FJs composed of two dissimilar solutions or even two immiscible liquids. Each of the two microfluidic lines can be independently biased via the connection of DC power sources (Delta Elektronika ES 0300) to embedded titanium electrode sheaths located 33 mm upstream of the impingement point. These voltage supplies allowed the application of up to ±300 V on each microjet prior to impingement. We monitored the applied potentials using voltmeters (Fluke 289 and Keithley 199) connected in parallel to each solution line. The precision of the voltmeters was ±0.01 V below 200 V and ±0.1 V above. These electrode sheaths also enabled grounding of the solutions when no bias voltage was desired. The entire FJ assembly can be rotated about its downstream axis (y-axis, as shown in Fig. 1), thereby enabling angle-dependent measurements with respect to the liquid surface, e.g., for depth-probing applications as mentioned earlier. Rotation also changes the illuminated/probed area with respect to the incident radiation and the detector, respectively.

We primarily conducted FJ-PES experiments at the U49-2_PGM-1[41] and UE-52_SGM[42] beamlines at the BESSY II synchrotron light facility in Berlin. Here, the entire FJ assembly was mounted via a rotatable *xyz*-manipulator onto the SOL^{3}PES endstation.[43] The measurements of organic-aqueous FJs were conducted at the P04 beamline[44] at the PETRA III synchrotron light facility in Hamburg, utilizing our custom experimental setup EASI (Electronic structure from Aqueous Solutions and Interfaces).[16] Prior to PES measurements, we adjusted the alignment (relative position) of the two impinging jets and considered the jets to be well aligned when the resulting FJ face lies entirely in the plane perpendicular to that defined by the microjets prior to impingement. To align the center of the FJ relative to the detection system, we oriented the first FJ leaf to the desired measurement angle (in our case, generally, θ_{leaf} = 45°, except for measurements conducted at P04, where θ_{leaf} was set to 0°; see Ref. 16 for details). We then swept the FJ perpendicular to the light axis until we identified the leaf edges on each side by monitoring the rapidly decreasing liquid-phase water $1b_1$ signal intensity. Finally, we maneuvered to the midpoint location between the identified rim positions.

To characterize the electric potential on either face of the FJ as a function of the applied bias voltage, we took advantage of the direct relationship between the applied sample bias and the shift in the as-measured kinetic energy of emitted photoelectrons. As discussed in detail in our previous work,[39] the application of a negative electric potential V_{Acc} to a liquid microjet of sufficiently conductive solution leads to a rigid shift of all liquid PE features on the as-measured kinetic-energy scale relative to a grounded sample, i.e., the photoelectrons accelerate in the electric field between the liquid jet and the analyzer orifice. Note that the potential difference between the jet and the analyzer can be of a smaller magnitude than the externally applied voltage (e.g., by a power source) due to internal resistances resulting in potential gradients between the outlet and the *in vacuo* liquid surface. The change in the kinetic energy relative to a grounded sample with V_{Acc} = 0 V (or spectral shift, as we denote it here) is, thus, a direct measure of the potential experienced by the sample at the location of photoionization.

For measurements involving organic liquids, we utilized commercial pre-fabricated microfluidic borosilicate chip nozzles (Micronit BV) with three individual colliding channels: two outer 40 μm channels at an impingement angle of 80° and one central bisecting 20 μm channel. These nozzles were used as all three channels can be run in the impingement mode simultaneously, a

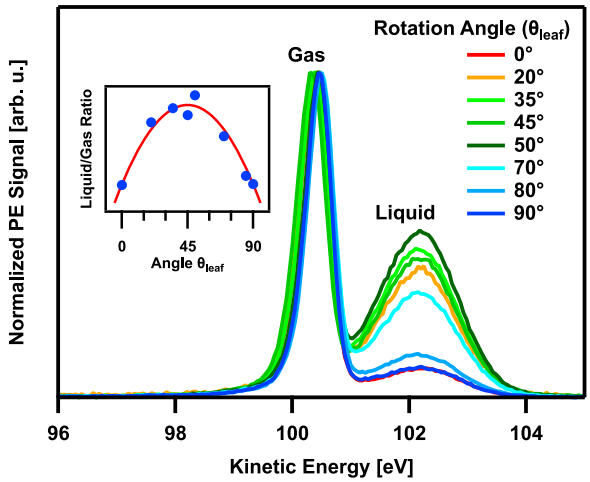

FIG. 2. Oxygen 1s photoelectron spectra obtained from a 30 mM NaCl aqueous flatjet as a function of rotation angle θ_{leaf} (defined in Fig. 1), featuring signal contributions from both the gas and liquid phases. We first maneuvered the ionization point to the center of the first leaf and then conducted measurements at different angles. The inset figure plots the liquid-to-gas signal ratio as a function of θ_{leaf} in degrees. A $\sin(\theta)$ function is a good fit to the data and can be seen as a trade-off between the surface component exposed to the light beam and to the detector axis. Thus, the highest ratio of liquid- to gas-phase peak areas was found when the flatjet face was oriented at an angle between the incident light and the analyzer, which in this case corresponded to θ_{leaf} = 45°. All measurements were conducted at $h\nu$ = 640 eV photon energy with both single jets electrically grounded. Spectra were aligned to the liquid-phase $1b_1$ peak position to emphasize the small apparent differences in the gas-phase $1b_1$ peak position, potentially caused by the inhomogeneous electric field between the grounded jet and the electron analyzer resulting from the anisotropic target geometry.

necessary capability for experiments involving encapsulated solutions,[45] as discussed below.

For the perpendicular arrangement of the photon beam and analyzer axis primarily employed in these experiments, we found that the rotation angle that maximizes the liquid-phase to gas-phase signal ratio corresponds to the angle at which the surface of the FJ lay in between the axis of light propagation and the detector (see Fig. 2); this happens to be approximately $\theta_{leaf} = 45°$ in the arrangement shown in Fig. 1. Although we attempted to control for positional drift accompanying the rotation of the FJ by monitoring the jet position using cameras at each angle, the actual position on the jet being probed was likely slightly different for each angle. Nevertheless, given the large beam spot size used for these measurements (larger than the width of the FJ leaf), we anticipate that the positional drift had a minor influence on the observed liquid- to gas-phase signal ratio. Note that the optimal orientation will depend on the specifics of the desired measurement. Here, we optimized for maximum liquid-phase to gas-phase signal to showcase the signal dependence on the rotation angle, but one might want, instead, to look at shallow surface species where a grazing angle of incidence might be preferred. Similarly, the configuration used in this work would not be ideal for studies of molecular orientation on the FJ surface. Whatever the case, the clear communication of this rotation angle will be critical for subsequent FJ-PES work to enable comparison between different studies.

III. RESULTS AND DISCUSSION

A. Mixing within a flatjet

The production of a FJ by the impingement of two cylindrical LJs of different solutions immediately raises the question of where along the FJ and on which time scales these solutions mix. We recently employed optical means to measure chemiluminescence upon impingement of two reacting aqueous solutions (luminol and hydrogen peroxide) using a comparable FJ assembly (with 50 μm inner diameter microjets, likely yielding a slightly thinner leaf compared to the 64 μm inner diameter jets used in the present work).[20] These experiments revealed that mixing between the two solutions in the first leaf is minimal and suggested that a FJ formed by the impingement of two different solutions can reasonably be thought of as two co-flowing laminar sheets sharing a liquid–liquid interface, which becomes slightly less defined along the length of the leaf as interdiffusion takes place. In contrast, on the rims of the first leaf and in the entirety of the second leaf, substantial turbulent mixing occurs. While these insights are generally valuable, it is important to keep in mind for the present work that the chemiluminescence that we observed upon the mixing of luminol and hydrogen peroxide aqueous solutions was inherently sensitive to the liquid–liquid interface and provided little information regarding the degree of interdiffusion and mixing near the liquid–vapor interfaces of the FJ. Due to the short mean free path of photoelectrons generated by the soft X-ray radiation used in our present work, our FJ-PES measurements are surface sensitive and probe only the first few nanometers into the liquid. These two approaches, thus, probe distinct yet complementary regions of the FJ.

To assess whether mixing at the liquid–liquid interface can affect the near-surface region probed by PES, we generated a mixed FJ using two different aqueous solutions. The first was a low-concentration (25 or 50 mM) NaCl(aq) solution containing just enough electrolyte to be conductive for biasing (this solution is spectrally indistinguishable from neat water and will be referred to as "neat water" throughout). This small salt concentration served to compensate for the streaming potential of the liquid jet, associated with charge build-up resulting from unequal shearing of the inner and outer Helmholtz layers along the liquid–solid interface within the microfluidic tubing prior to injection into vacuum.[46,47] The second solution was a high-concentration (1 or 2 M) NaI(aq) solution with distinctive solute PES features separate from the valence band of water. In particular, Na 2p and I 4d features appear at 38 and 55 eV binding energies, respectively.[48] We measured the valence-band PE spectra ($h\nu$ = 310 eV) from the middle of both faces of the first and second leaves of this mixed FJ, looking for NaI signatures on the low-concentration face that would indicate mixing or significant interdiffusion within the nanometer-scale probing depth near the liquid–vapor interface. To ensure identical probing in the center of the FJ leaf on both faces, we interchanged the sample solution lines rather than physically rotating the jet by 180°.

As shown in the top panel of Fig. 3, solute features are completely absent in the spectrum measured at the water face. Note that PES is generally insensitive to small bulk concentrations (≤10 mM) unless the solute is strongly surface-active.[49] This demonstrates that mixing in the first leaf is negligible for PES applications. We repeated these measurements using 600 eV photon energy, corresponding to a probing depth of 2–4 nm,[30,50] with the same result. In the second leaf, however, signatures of NaI(aq) were found on both faces with comparable intensity (Fig. 3, bottom panel).

Based on our recently developed method of calibrating FJ thickness using an IR camera, we estimate that the thickness of the FJ studied here was 3 μm in the middle of the first leaf,[51] where we conducted FJ-PES measurements. While the present measurements did not reveal any spectroscopic signatures of interdiffusion near the liquid–vapor interfaces at this location, such interdiffusion would likely significantly affect the surface concentration of solute in a much thinner FJ leaf. This could open up the possibility to study reactions at the liquid–liquid interface by simply scanning the first leaf along its length.[38] For now, we provide a simple estimate of the concentration of NaI at the NaCl face, using the relation for one-dimensional diffusion, as derived from Fick's second law,

$$n(x,t) = \frac{n_0}{2}\,\mathrm{erfc}\left(\frac{x}{2\sqrt{Dt}}\right), \tag{1}$$

with x denoting the spatial distance from the liquid–liquid interface at $x = 0$ and t denoting the time. As mentioned above, we estimate the FJ thickness to be 3 μm, resulting in a distance of $x = 1.5$ μm between the liquid–liquid interface and the FJ surface. The initial source concentration n_0 was 2 M on the NaI face ($x < 0$). The fluid velocity was estimated as 15 m/s, calculated from an HPLC pumping rate of 3 ml/min and a jet-nozzle diameter of 64 μm. At the measurement location, ~1 mm below the impingement point, this corresponds to a diffusion time of roughly 70 μs. The diffusion constants D of Na^+ and I^- ions in water are ~2×10^{-5} cm^2/s (at 25 °C).[52] Using these values, we calculate a small surface concentration of less than 10 mM at the NaCl face, which is below our detection threshold under the employed measurement conditions.

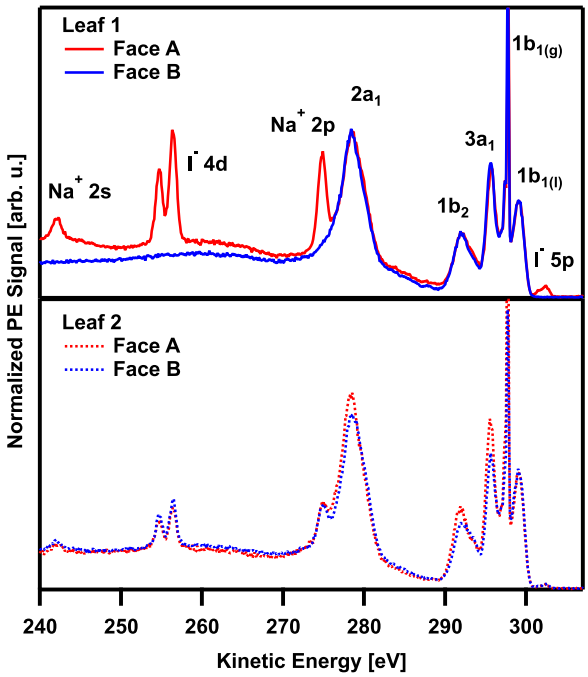

FIG. 3. Photoelectron spectra obtained from either face of a 2 M NaI (Face A) / neat water (Face B) aqueous flatjet at the center of both the first (top) and second (bottom) leaves. Mixing in the first leaf is below detection threshold as observed by the absence of solute features on the neat-water face, whereas in the second leaf, signatures of NaI are observed on both faces with approximately equal signal strength, indicating complete mixing from the first node (above the second leaf) onward. Spectra obtained from either face were normalized to the liquid water $1b_1(l)$ signal. The larger background signal apparent in the Face A spectrum compared to the Face B spectrum from the first FJ leaf is due to the scattering of Na^+ 2p, Na^+ 2s, and I^- 4d photoelectrons in solution. As the second leaf is perpendicular to the first, the naming convention is arbitrary, i.e., the jet was simply rotated +90° with respect to measurements of the first leaf. All water valence and solute core-level contributions are assigned in the top panel. All measurements were conducted with $h\nu$ = 310 eV photons and an electrically grounded flatjet.

Note that our estimation does not capture the full complexity of the system. The flow-rate estimation does not account for the impingement angle of the jets used. In reality, following impingement, only a $\cos(\phi/2)$ component (where ϕ is the impingement angle) of the fluid velocity is in the direction of fluid flow. More importantly, we know from infrared-camera measurements that the FJ cools rapidly in vacuum, with a temperature of about 15 °C, 1 mm below the impingement point, rather than the initial sample temperature of 25 °C.[53,54] This indicates that the diffusion of ions would likely be slower than we have assumed. We also ignore the reality of NaCl diffusion from the water into the NaI sheet. Nevertheless, given that the estimated concentration here is on the order of what can be detected with PES, we anticipate that a much thinner jet would exhibit detectable levels of interdiffusion, even in the first leaf, if the solution concentrations are high enough. Repeating the same calculation for a FJ with a total leaf thickness of 1 μm yields an expected surface concentration of NaI on the water face of a few hundred mM, which would be easily detectable.

B. Biasing of a flatjet

Having confirmed that mixing between the two solutions is minimal within the first leaf and that the FJ is composed of two free-flowing sheets with a shared liquid–liquid interface, we attempted to generate a measurable potential gradient across the FJ leaf by applying a different bias voltage to each solution line prior to impingement. Here, we define V_{Acc}^{A} and V_{Acc}^{B} as the accelerating voltages applied to the solution lines that constitute Face A and Face B of the FJ following impingement (with respect to the analyzer), respectively. It is important to note that these voltages are not applied directly to the faces but rather 33 mm upstream, as detailed earlier. In addition, we introduce two additional terms that will be useful for the analysis of asymmetrically applied voltages; $\Delta V_{Acc} = |V_{Acc}^{A} - V_{Acc}^{B}|$ is the magnitude of the difference in voltages applied to the microjets constituting Face A and Face B of the FJ, and eU_{Eff} is the spectral shift (in eV) measured at the FJ and is the representative of the local electrical potential at the surface of the first leaf. We clarify that we use eU_{Eff} rather than V_{Eff} because we are not directly measuring a voltage at the surface but rather inferring a potential based on a change in the kinetic energy of water's $1b_1$ feature relative to the reference case of a grounded FJ with $V_{Acc} = V_{Acc}^{A} = V_{Acc}^{B} = 0$ V.

As is the case for a cylindrical LJ, the application of a symmetric bias voltage ($V_{Acc} = V_{Acc}^{A} = V_{Acc}^{B}$) to a FJ causes a spectral shift (eU_{Eff}) that scales linearly with the applied bias voltage [Fig. 4(a)]. In addition, the gaseous water $1b_1$ signal decreases in intensity and broadens with increasing applied bias [Fig. 4(b)]. These trends are consistent with measurements from biased cylindrical jets and have extensively been discussed in earlier works.[39,40,54] The small differences in bias-voltage-subtracted peak position in Fig. 4(b) are within the error of applied voltages (see Sec. II for more details on the precision of the power sources). Photoelectrons originating from the gas phase experience only a fraction of the net accelerating field between the liquid surface and the analyzer orifice, depending on the exact location of ionization; thus, gas-phase signals are shifted somewhat less and significantly broadened upon biasing. At significantly high applied bias voltages, the gas-phase signal contribution is completely smeared out and an essentially gas-free liquid PE spectrum can be obtained. A closer look at the bias-voltage-subtracted spectra in Fig. 4(b) reveals that, in this case, an accelerating voltage of approximately −80 V was necessary to completely suppress the gas-phase signal (at around 12.6 eV, seen as a sharp dip between the liquid $1b_1$ and $3a_1$ features), which is much higher than is typically necessary for cylindrical LJs. This is likely due to the lack of surface curvature, which in combination with a high surface area leads to a large vapor density directly above the liquid surface, where almost the full potential gradient acts on photoelectrons from the gas phase.

For a FJ generated from two independent LJs, the question of applying asymmetric bias voltages ($V_{Acc}^{A} \neq V_{Acc}^{B}$) naturally arises. Holding V_{Acc}^{B} constant at −50 V and setting V_{Acc}^{A} to −250 V results in ΔV_{Acc} = 200 V (here, V_{Acc}^{B} is chosen for convenience but has no influence on the result as we see later, i.e., only ΔV_{Acc} is relevant). Measuring valence-band photoelectron (PE) spectra in this configuration from both faces of the FJ in the middle of the first leaf revealed that, within the error of our measurement, there was no difference in eU_{Eff} as measured from Face A vs from Face B, i.e., the relative shift in kinetic energy was indistinguishable ($U_{Eff}^{A} = U_{Eff}^{B}$).

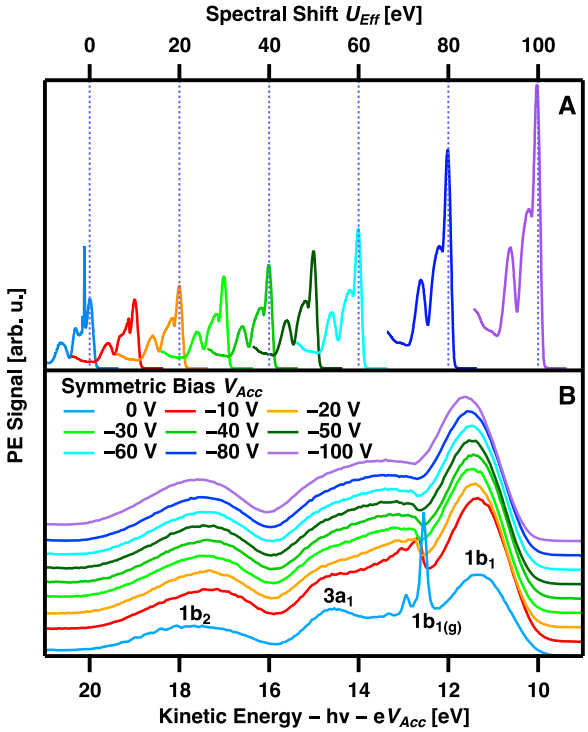

FIG. 4. Measured valence-band spectra for a FJ composed of a 30 mM aqueous solution of NaCl as a function of symmetrically applied bias. Analogously to cylindrical jets, the water valence band shifts (a) and the gas-phase signal is suppressed (b) proportionally to the magnitude of the negative potential applied. The observed increase in PE signal upon bias application also occurs in experiments with cylindrical jets and is likely due to a focusing effect of the negative potential, drawing electrons toward the analyzer orifice. The bottom spectra have been normalized to the liquid water $1b_1$ signal intensity and are offset for clarity. All measurements were conducted with $h\nu$ = 150 eV photons.

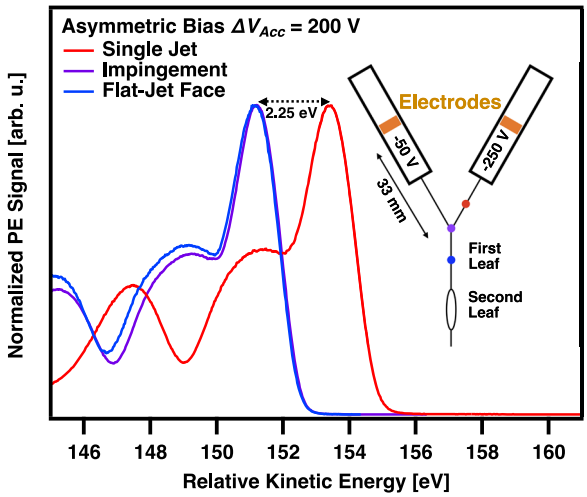

FIG. 5. Photoelectron spectra from a conductive aqueous flatjet (50 mM NaCl) under asymmetric biasing conditions. The bottom axis indicates the kinetic energy of liquid water $1b_1$ peak positions relative to a grounded-jet spectrum (V^A_{Acc} = −250 V, V^B_{Acc} = −50 V, and ΔV_{Acc} = 200 V) at different measurement positions: at a single jet prior to impingement (red), directly at the point of impingement (purple), and on the first FJ leaf (blue, see main text and inset). All measurements were conducted with $h\nu$ = 150 eV photons. The sketch of quartz capillaries with embedded electrodes, cylindrical microjets, and the resulting flatjet in the inset is not drawn to scale.

This indicates that the applied voltage is likely dropping along the solution lines rather than across the FJ leaf, as a large voltage drop across the FJ would lead to a difference in potential observed on each face. To better understand the voltage evolution from the points of application, we measured eU_{Eff} at three different locations using the same applied biases: first at microjet A prior to the point of impingement, then at the point of impingement, and finally at Face A of the FJ (Fig. 5, red, purple, and blue traces, respectively). We observe a somewhat larger value of eU_{Eff} of a few eV prior to impingement, while the impingement point and the Face A of the FJ appear to be at the same potential. These measurements confirm that the bias voltage drops almost entirely along the individual cylindrical jets, with only a small fraction likely to drop across the FJ leaf itself. We note that, although the solutions studied are ionically conductive, we do not anticipate that the applied voltages will drive net ion transport between the two electrodes. The drift velocity of the ions under the studied conditions is on the order of hundreds of μm/s,[52] while the solution velocity is on the order of tens of m/s. Rather, the current is likely driven by charge transfer at the titanium electrodes.

To fully characterize the voltage drop from the titanium electrodes to the FJ, we conducted a series of eU_{Eff} measurements with different asymmetric bias voltages (0 V ≤ΔV_{Acc} ≤ 250 V) for mixed FJs composed of either low-conductivity 25 mM NaCl(aq), high-conductivity 1 M NaI(aq), or a combination thereof. This resulted in four distinct (Face A/Face B) FJ configurations, for which the results are summarized in Fig. 6: (1) 1 M NaI/1 M NaI (red circles), (2) 25 mM NaCl/25 mM NaCl (blue circles), (3) 1 M NaI/25 mM NaCl (green triangles), and (4) 25 mM NaCl/1 M NaI (black triangles). All measurements of eU_{Eff} were conducted using Face A. In each case, we found that U^A_{Eff} scales linearly with ΔV_{Acc} and that the slope of the relationship is determined by the ratio of the conductivities of the solutions on the two faces of the FJ. For the homogeneous FJs—(1) and (2)—U^A_{Eff} was the average of the two applied bias voltages. No differences were observed to arise due to the differences in the net conductivity for these FJs. For the heterogeneous FJs—(3) and (4)—the bias voltage applied to the more conductive solution line determined U^A_{Eff} nearly entirely, regardless of the bias voltage applied to the other solution line. This can be seen from the steep slope when measuring from (3), while the slope of (4) is nearly zero, indicating that the majority of the voltage is dropping across the less conducting solution line.

These results are not surprising when picturing the FJ as a set of resistors in series with a net applied voltage of ΔV_{Acc}. In our experiment, the bias voltage was applied via titanium electrodes in contact with the liquid roughly 33 mm upstream of the impingement point outside of the vacuum chamber; the liquid has no contact with any metallic surface beyond this point. The entire circuit can then be considered as three elements in series— constituting the two solution lines and the impinging region/FJ— each with an associated impedance. Given the geometry of the system, the relatively short impinging region should constitute a vanishingly small part

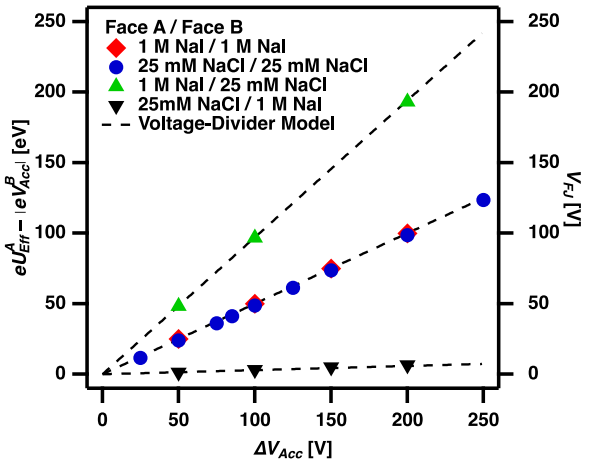

FIG. 6. Spectral shift eU^A_{Eff} measured at Face A of the flatjet (FJ), compensated for the minimum applied voltage of V^B_{Acc}, of the water $1b_1$ peak position for various compositions of homogeneous and heterogeneous aqueous FJs under different asymmetrically applied bias conditions. The slope of the relationship between spectral shift and difference in applied bias is entirely dependent on the ratio of the solution conductivities. The dashed lines were calculated using Eq. (2) and experimentally determined conductivity values. For all of these measurements, V^B_{Acc} was held at a constant value of −50 V such that a value of $\Delta V_{Acc} = 0$ V corresponds to $V^A_{Acc} = V^B_{Acc} = -50$ V.

of the total system impedance and, to a first approximation, may be neglected. Assuming that the system behaves in accordance with Ohm's law, the FJ can be modeled as the midpoint of a basic two-element voltage divider. As the electrolyte solutions are conductive and constantly replenished, and there are no expected capacitive contributions, the system may be treated as a purely resistive voltage divider, with R^A and R^B corresponding to the resistance of the two solution lines. If the solution lines are of equal length (from the point of voltage application to the impingement point) and inner diameter, then the resistivity (inverse of the conductivity) of each solution may be substituted for each element. In this case, the expected voltage measured at the impinging point or at the first leaf of the FJ (as seen from Face A) is given by

$$V_{FJ} = \frac{-\rho^A}{\rho^A + \rho^B}\Delta V_{Acc} - V^B_{Acc}, \tag{2}$$

where ρ^A and ρ^B correspond to the resistivity of the solutions that constitute Face A and Face B of the FJ, respectively, and $\Delta V_{Acc} = |V^A_{Acc} - V^B_{Acc}|$ as defined above. For homogeneous FJs ($\rho^A = \rho^B$), the equation simplifies to $V_{FJ} = -\frac{1}{2}\Delta V_{Acc} - V^B_{Acc}$. To calculate the expected V_{FJ} for the heterogeneous case, the relative resistivities/conductivities of the solutions used must be known. We measured the 1 M NaI solution to be 31 times as conductive as the 25 mM NaCl solution. The calculated values of V_{FJ} based on measured conductivities are overlaid on the measured eU_{Eff} data in Fig. 6 and demonstrate excellent agreement, indicating that the mixed FJ may indeed be accurately modeled as a voltage divider. Considering the thickness of the FJ relative to the distance between the electrodes (3 μm vs 66 mm), and assuming a linear voltage drop across the system with $\Delta V_{Acc} = 200$ V, we would expect a difference in eU_{eff} of ~10 meV as measured from Face A and Face B. The resolution of such small energetic differences pushes the limits of LJ-PES and was not possible in the present study.

Additional challenges preclude the observation of effects of such magnitude at the moment. If one is simply to switch the applied voltages V^A_{Acc} and V^B_{Acc} to measure eU_{Eff} from each face, it must be assumed that each solution line is of the exact same length and inner diameter such that the FJ is at exactly the resistive center of the circuit. However, the resistive path length may be slightly different depending on the exact distance between each titanium electrode sheath and the impinging region, depending on the specific FJ assembly. We found that this effect alone can lead to an asymmetric potential drop toward one specific (physical) side of the FJ assembly, i.e., the spectral shift is always a bit larger on one side, independent of the biasing configuration or solution. This strongly hints at intrinsic, unequal resistive paths on each side of the assembly. Indeed, this is shown in Fig. 5, where the relative kinetic energy of the spectrum measured at Face A of the FJ is 151 eV rather than 150 eV, as would be expected if both sides of the assembly were equally resistive.

It is challenging to ensure equal length in solution lines at the required few-micron scale, to not even mention the manufacturing tolerances of the PEEK tubing used and the precision of the voltmeters. Thus, the measurements of effective bias voltages should be checked by using both sides of a FJ to circumvent systematic errors, i.e., one must physically rotate the FJ by 180° about its axis. However, unless the flow axis is exactly centered and perpendicular to both the light-propagation and detection axes, such a rotation will inevitably lead to offsets in the measured position from each side. While the FJ can be subsequently realigned to minimize this effect, we observed that even very small changes in the measured position can lead to shifts in the measured value of eU_{Eff} on the order of 100 meV, likely due to the inhomogeneity of the potential-energy landscape above the FJ as a consequence of its unusual shape.

Nevertheless, these challenges are not insurmountable in the long term, and we close this section by discussing possible applications of asymmetric biasing and ideas for how a larger potential gradient across the FJ leaf could be generated and detected. A simple approach would be to increase the relative impedance of the FJ with respect to the total impedance of the circuit, e.g., by shortening the length of the entire circuit, such that the FJ thickness constitutes a large fraction of the path length between the two electrodes. For example, if the length between electrodes could be shortened to 6 mm, the expected linear voltage drop across the FJ would increase correspondingly to 100 mV. This would correspond to a voltage gradient of ~300 V/cm across a 3 μm thick FJ leaf, which, while significant, is still well below the anticipated voltage gradient of $>10^7$ V/cm required for the static orientation of water molecules near room temperature.[55,56] In addition, this approach clearly has geometric limits. Another interesting approach would be to alter the characteristics of the circuit to achieve the equivalent of a sandwich-style FJ in which one central layer has a much higher impedance than the outer two layers. We will discuss this approach in greater detail below. In addition to potential-induced orientation in molecules at the liquid–vapor or liquid–liquid interface, as discussed earlier, a larger voltage difference could be used to drive increased ion diffusion across the liquid–liquid interface, which could be used to tune reaction kinetics if two reacting solutions are impinged.

C. Aqueous–organic solution interfaces

Having independent control of two distinct free-flowing sheets may be exceptionally useful in the study of ionically mobile species in solution and, in particular, for complex or amphiphilic species, or for phase-transfer catalysts, in the instance where one of the aqueous solutions is substituted by an organic liquid.[57–60] In particular for chiral phase-transfer catalysts, which are critical for determining the stereospecificity of chiral reaction products, open questions remain regarding the degree to which ion-pairing or hydrogen-bonding mechanisms dominate or coexist in directing reagents, and correspondingly, the protonation state of reaction intermediaries is not well understood.[61] Such systems are not often investigated using vacuum-based UV or x-ray spectroscopy, in large part due to the general difficulty of preparing stable aqueous–organic interfaces in vacuum. Instead, reactant yield is often used as a primary metric, and catalytic mechanisms are subsequently inferred. In principle, however, chemical activity at the liquid–liquid interface should be accessible by employing liquid-FJ techniques in combination with photon-out spectroscopic methods (such as XAS), scattering-based approaches,[62] or, if the FJ can be made sufficiently thin, PES.

In the context of generating potential gradients across the liquid–liquid interface, organic–aqueous FJs also constitute a unique avenue toward locally tuning the FJ impedance relative to that of the entire system. Recently, the generation of aqueous–organic–aqueous and organic–aqueous–organic sandwich-style heterostructures has been demonstrated through the impingement of three cylindrical microjets.[45] Two jets are run in the standard impingement configuration, with a third in the plane of the FJ (bisecting the angle between the other two). If the outer jet solutions are miscible with one another but not with the middle jet solution, then the inner solution can be encapsulated as a sheet within the outer solutions. If, for example, a high-impedance thin film of an organic liquid were introduced between two aqueous sheets (or vice versa), the local impedance within the FJ will change relative to the total impedance of the circuit. To determine the encapsulating behavior of such FJs, we generated a toluene-aqueous solution-toluene FJ heterostructure and conducted core-level PES measurements on the outer surface of the FJ leaf, looking for (toluene-originating) carbon and (water-originating) oxygen signatures. The results of these measurements are shown in Fig. 7. With the toluene enveloping the aqueous solution, the spectra revealed traces of neither liquid nor gaseous water oxygen 1s core-level signals, indicating that there was no leakage of water from between the toluene sheets and that not even water vapor could escape encapsulation.

By moving the jet away from the ionization point and, thus, exposing only the vapor layer surrounding the jet, we were able to measure the pure gas C 1s toluene spectrum. We noted a 300 meV energy shift in the gas-phase C 1s peak position between the gas-only and the liquid-and-gas spectra, indicating that some surface charging may occur upon photoionization of the non-conductive toluene. This is expected given that toluene is electrically insulating, and we did not add any salt to the sample prior to the measurement (due to the poor solubility of common salts in toluene). We note that pure water exhibits a pronounced charge-up when exposed to synchrotron radiation as well, actually leading to unstable and broadened spectra.[39] It is rather surprising that the observed shift due to charge-up in toluene is so small and that it was possible to measure a stable spectrum from the insulating liquid directly. One may speculate that charge compensation is provided by the highly conductive aqueous solution inside the core of the FJ, which provides a kind of back contact; however, the exact mechanisms enabling these experiments remain unclear at the moment. Nevertheless, some precedent exists for this behavior and it was previously found that other insulating organic liquids, for example, nonane and benzene, also yield well-defined PE spectra without requiring the addition of salt.[1,5] Our results demonstrate the ability to generate a stable FJ with a well-defined liquid–liquid interface even from two immiscible liquids with different physical properties. We are currently building upon this approach to develop a biased version of such a sandwich structure, which we anticipate will be a critical element for the generation of a measurable potential gradient across the FJ.

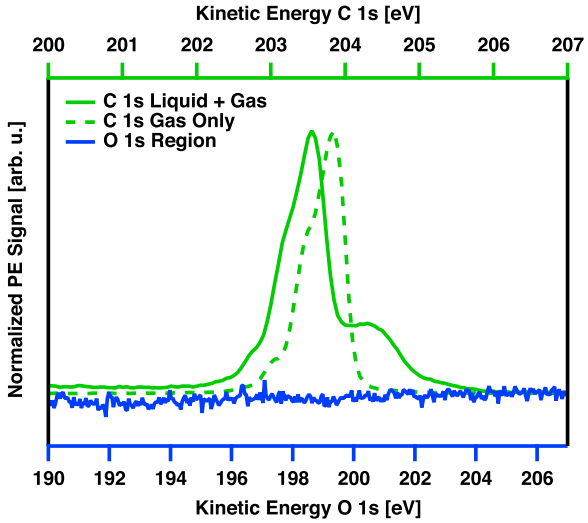

FIG. 7. Core-level photoelectron spectra obtained from a toluene–1 M NaCl(aq)–toluene encapsulated flatjet. O 1s (blue) and C 1s (green) spectra were measured with $h\nu$ = 738 eV and $h\nu$ = 495 eV photons, respectively, ~200 eV above the threshold ionization energy in each case. The gas-only toluene spectrum was measured by moving the flatjet out of the path of the synchrotron radiation such that only gaseous molecules were photoionized. Whereas the C 1s signal is clearly present for both liquid- and gas-phase toluene, O 1s signal originating from the encapsulated solution is completely absent. All measurements were done with electrically grounded solutions.

IV. CONCLUSIONS

We have demonstrated the versatility of FJ-PES to study free-flowing liquid flatjets, formed through the impingement of two independent cylindrical jets in vacuum. We have reported PE spectra from mixed FJs and found that the two faces of the first FJ leaf retain the characteristics of the individual impinging jets. While some interdiffusion is likely to take place along the liquid–liquid interface within the FJ, the concentration of diffused ions is below the detection limit of PE spectroscopy within the surface region probed but may be greatly increased if the FJ were made thinner. In contrast, we found that the second leaf of the FJ is homogeneously

mixed. These observations highlight FJs as an attractive experimental target for the study of chemical dynamics in systems of reacting solutions, especially those with fast reaction kinetics.

We have also conducted experiments with asymmetrically biased FJs, where we applied a different bias voltage to each of the two cylindrical jets prior to impingement. Our work reveals that the voltage drop across the individual solution lines up until the point of impingement is largely determined by the ratio of the conductivities of the two solutions impinged and that the entire system is electrically equivalent to a voltage divider. We were unable to observe a potential gradient across the FJ (defined as a different effective potential measured at either face) under present conditions; however, we hypothesize that with improvements to the FJ, such a gradient could be generated and observed. Given that the application of an asymmetric bias across the FJ should drive an ionic current across the thickness of the FJ leaf, such a system may be useful for the characterization of ionically mobile species in solution, in particular for complex ions or amphiphilic species.

Finally, we have demonstrated the generation of stable FJs composed of immiscible liquids in impingement. Due to the minimal degree of interdiffusion between immiscible liquids, the liquid–liquid interface in these FJs should be especially stable. Such FJs constitute a unique template, enabling the application of x-ray-based techniques to elucidate phase-transfer mechanisms or identify evidence of interfacial molecular orientation or accumulation.

ACKNOWLEDGMENTS

The authors thank the mechanical workshop of the Fritz-Haber-Institute (FHI) and the Helmholtz-Zentrum Berlin (HZB) staff for their assistance prior to and during the beamtime at BESSY II, as well as Aaron M. Ghrist for his assistance with preliminary measurements. The authors also acknowledge the beamtime at BESSY II provided through user proposals under Grant Nos. 191-08169, 221-11064, and 222-11554, and at PETRA III provided through a user proposal under Grant No. II-20210015. B.W. acknowledges the support from the Deutsche Forschungsgemeinschaft (Grant No. Wi 1327/5-1). F.T. and B.W. acknowledge the support by the MaxWater initiative of the Max-Planck-Gesellschaft. D.S., T.B., K.M., M.P., B.C., U.H., and B.W. acknowledge the funding from the European Research Council (ERC) under the European Union's Horizon 2020 research and investigation program (Grant Agreement No. 883759). BC acknowledges the funding from the EPFL-MPG doctoral school. S.T. acknowledges the support from JSPS KAKENHI Grant No. JP20K15229.

AUTHOR DECLARATIONS

Conflict of Interest

The authors have no conflicts to disclose.

Author Contributions

Dominik Stemer: Conceptualization (equal); Formal analysis (lead); Investigation (equal); Writing – original draft (equal); Writing – review & editing (equal). **Tillmann Buttersack**: Conceptualization (equal); Formal analysis (equal); Investigation (equal); Writing – review & editing (equal). **Henrik Haak**: Conceptualization (equal); Investigation (equal); Writing – review & editing (equal). **Sebastian Malerz**: Conceptualization (equal); Investigation (equal); Writing – review & editing (equal). **Hanns Christian Schewe**: Formal analysis (equal); Investigation (equal); Writing – review & editing (equal). **Florian Trinter**: Investigation (equal); Writing – review & editing (equal). **Karen Mudryk**: Investigation (equal); Writing – review & editing (equal). **Michele Pugini**: Investigation (equal); Writing – review & editing (equal). **Bruno Credidio**: Investigation (equal); Writing – review & editing (equal). **Robert Seidel**: Investigation (equal); Writing – review & editing (equal). **Uwe Hergenhahn**: Investigation (equal); Supervision (equal); Writing – review & editing (equal). **Gerard Meijer**: Supervision (equal); Writing – review & editing (equal). **Stephan Thürmer**: Conceptualization (equal); Formal analysis (equal); Investigation (equal); Supervision (equal); Writing – review & editing (equal). **Bernd Winter**: Conceptualization (equal); Investigation (equal); Supervision (equal); Writing – review & editing (equal).

DATA AVAILABILITY

The data that support the findings of this study are openly available in Zenodo at http://doi.org/10.5281/zenodo.7806035.

REFERENCES

[1] M. Faubel, B. Steiner, and J. P. Toennies, J. Chem. Phys. **106**, 9013 (1997).
[2] B. Winter, R. Weber, W. Widdra, M. Dittmar, M. Faubel, and I. V. Hertel, J. Phys. Chem. A **108**, 2625–2632 (2004).
[3] T. Buttersack, P. E. Mason, R. S. McMullen, T. Martinek, K. Brezina, D. Hein, H. Ali, C. Kolbeck, C. Schewe, S. Malerz, B. Winter, R. Seidel, O. Marsalek, P. Jungwirth, and S. E. Bradforth, J. Am. Chem. Soc. **141**, 1838–1841 (2019).
[4] S. Thürmer, T. Shinno, and T. Suzuki, J. Phys. Chem. A **125**, 2492–2503 (2021).
[5] H. C. Schewe, K. Brezina, V. Kostal, P. E. Mason, T. Buttersack, D. M. Stemer, R. Seidel, W. Quevedo, F. Trinter, B. Winter, and P. Jungwirth, J. Phys. Chem. B **126**, 229–238 (2022).
[6] I. Unger, R. Seidel, S. Thürmer, M. N. Pohl, E. F. Aziz, L. S. Cederbaum, E. Muchová, P. Slavíček, B. Winter, and N. V. Kryzhevoi, Nat. Chem. **9**, 708–714 (2017).
[7] T. Jahnke, U. Hergenhahn, B. Winter, R. Dörner, U. Frühling, P. V. Demekhin, K. Gokhberg, L. S. Cederbaum, A. Ehresmann, A. Knie, and A. Dreuw, Chem. Rev. **120**, 11295–11369 (2020).
[8] I. Unger, D. Hollas, R. Seidel, S. Thürmer, E. F. Aziz, P. Slavíček, and B. Winter, J. Phys. Chem. B **119**, 10750–10759 (2015).
[9] B. Winter, M. Faubel, R. Vácha, and P. Jungwirth, Chem. Phys. Lett. **474**, 241–247 (2009).
[10] R. Dupuy, J. Filser, C. Richter, R. Seidel, F. Trinter, T. Buttersack, C. Nicolas, J. Bozek, U. Hergenhahn, H. Oberhofer, B. Winter, K. Reuter, and H. Bluhm, Phys. Chem. Chem. Phys. **24**, 4796–4808 (2022).
[11] R. Dupuy, C. Richter, B. Winter, G. Meijer, R. Schlögl, and H. Bluhm, J. Chem. Phys. **154**, 060901 (2021).
[12] R. Dupuy, J. Filser, C. Richter, T. Buttersack, F. Trinter, S. Gholami, R. Seidel, C. Nicolas, J. Bozek, D. Egger, H. Oberhofer, S. Thürmer, U. Hergenhahn, K. Reuter, B. Winter, and H. Bluhm, Phys. Rev. Lett. **130**, 156901 (2023).
[13] B. Winter and M. Faubel, Chem. Rev. **106**, 1176–1211 (2006).
[14] R. Seidel, B. Winter, and S. E. Bradforth, Annu. Rev. Phys. Chem. **67**, 283–305 (2016).
[15] R. Signorell and B. Winter, Phys. Chem. Chem. Phys. **24**, 13438–13460 (2022).
[16] S. Malerz, H. Haak, F. Trinter, A. B. Stephansen, C. Kolbeck, M. Pohl, U. Hergenhahn, G. Meijer, and B. Winter, Rev. Sci. Instrum. **93**, 015101 (2022).

[17]D. Hasson and R. E. Peck, AIChE **10**, 752–754 (1964).
[18]J. W. M. Bush and A. E. Hasha, J. Fluid Mech. **511**, 285–310 (2004).
[19]M. Ekimova, W. Quevedo, M. Faubel, P. Wernet, and E. T. J. Nibbering, Struct. Dyn. **2**, 054301 (2015).
[20]H. C. Schewe, B. Credidio, A. M. Ghrist, S. Malerz, C. Ozga, A. Knie, H. Haak, G. Meijer, B. Winter, and A. Osterwalder, J. Am. Chem. Soc. **144**, 7790–7795 (2022).
[21]G. Galinis, J. Strucka, J. C. T. Barnard, A. Braun, R. A. Smith, and J. P. Marangos, Rev. Sci. Instrum. **88**, 083117 (2017).
[22]J. C. T. Barnard, J. P. Lee, O. Alexander, S. Jarosch, D. Garratt, R. Picciuto, K. Kowalczyk, C. Ferchaud, A. Gregory, M. Matthews, and J. P. Marangos, Front. Mol. Biosci. **9**, 1044610 (2022).
[23]D. J. Hoffman, T. B. Van Driel, T. Kroll, C. J. Crissman, E. S. Ryland, K. J. Nelson, A. A. Cordones, J. D. Koralek, and D. P. DePonte, Front. Mol. Biosci. **9**, 1048932 (2022).
[24]C. J. Crissman, M. Mo, Z. Chen, J. Yang, D. A. Huyke, S. H. Glenzer, K. Ledbetter, J. P. F. Nunes, M. L. Ng, H. Wang, X. Shen, X. Wang, and D. P. DePonte, Lab Chip **22**, 1365–1373 (2022).
[25]J. D. Koralek, J. B. Kim, P. Brůža, C. B. Curry, Z. Chen, H. A. Bechtel, A. A. Cordones, P. Sperling, S. Toleikis, J. F. Kern, S. P. Moeller, S. H. Glenzer, and D. P. DePonte, Nat. Commun. **9**, 1353 (2018).
[26]Z.-H. Loh, G. Doumy, C. Arnold, L. Kjellsson, S. H. Southworth, A. Al Haddad, Y. Kumagai, M.-F. Tu, P. J. Ho, A. M. March, R. D. Schaller, M. S. Bin Mohd Yusof, T. Debnath, M. Simon, R. Welsch, L. Inhester, K. Khalili, K. Nanda, A. I. Krylov, S. Moeller, G. Coslovich, J. Koralek, M. P. Minitti, W. F. Schlotter, J.-E. Rubensson, R. Santra, and L. Young, Science **367**, 179–182 (2020).
[27]C. Lee, M. N. Pohl, I. A. Ramphal, W. Yang, B. Winter, B. Abel, and D. M. Neumark, J. Phys. Chem. A **126**, 3373–3383 (2022).
[28]I. V. Stiopkin, C. Weeraman, P. A. Pieniazek, F. Y. Shalhout, J. L. Skinner, and A. V. Benderskii, Nature **474**, 192–195 (2011).
[29]M. Bonn, Y. Nagata, and E. H. G. Backus, Angew. Chem., Int. Ed. **54**, 5560–5576 (2015).
[30]S. Thürmer, R. Seidel, M. Faubel, W. Eberhardt, J. C. Hemminger, S. E. Bradforth, and B. Winter, Phys. Rev. Lett. **111**, 173005 (2013).
[31]S. Gozem, R. Seidel, U. Hergenhahn, E. Lugovoy, B. Abel, B. Winter, A. I. Krylov, and S. E. Bradforth, J. Phys. Chem. Lett. **11**, 5162–5170 (2020).
[32]A. Schild, M. Peper, C. Perry, D. Rattenbacher, and H. J. Wörner, J. Phys. Chem. Lett. **11**, 1128–1134 (2020).
[33]M. F. Toney, J. N. Howard, J. Richer, G. L. Borges, J. G. Gordon, O. R. Melroy, D. G. Wiesler, D. Yee, and L. B. Sorensen, Nature **368**, 444–446 (1994).
[34]K.-i. Ataka, T. Yotsuyanagi, and M. Osawa, J. Phys. Chem. **100**, 10664–10672 (1996).
[35]Z. D. Schultz, S. K. Shaw, and A. A. Gewirth, J. Am. Chem. Soc. **127**, 15916–15922 (2005).
[36]A. Montenegro, C. Dutta, M. Mammetkuliev, H. Shi, B. Hou, D. Bhattacharyya, B. Zhao, S. B. Cronin, and A. V. Benderskii, Nature **594**, 62–65 (2021).
[37]K. Ray, A. Limaye, K. C. Ng, A. Saha, S. Shin, M.-P. Gaigeot, S. Pezzotti, A. Willard, and H. Allen, "Pushing and pulling on OH^- and H_3O^+ with electric fields across water's surface," chemRxiv:10.26434 (2022).
[38]P. Erni and A. Elabbadi, Langmuir **29**, 7812–7824 (2013).
[39]S. Thürmer, S. Malerz, F. Trinter, U. Hergenhahn, C. Lee, D. M. Neumark, G. Meijer, B. Winter, and I. Wilkinson, Chem. Sci. **12**, 10558–10582 (2021).
[40]B. Winter, S. Thürmer, and I. Wilkinson, Acc. Chem. Res. **56**, 77–85 (2023).
[41]T. Kachel, J. Large-Scale Res. Facil. **2**, A72 (2016).
[42]K. Godehusen, H.-C. Mertins, T. Richter, P. Zimmermann, and M. Martins, Phys. Rev. A **68**, 012711 (2003).
[43]R. Seidel, M. N. Pohl, H. Ali, B. Winter, and E. F. Aziz, Rev. Sci. Instrum. **88**, 073107 (2017).
[44]J. Viefhaus, F. Scholz, S. Deinert, L. Glaser, M. Ilchen, J. Seltmann, P. Walter, and F. Siewert, Nucl. Instrum. Methods Phys. Res., Sect. A **710**, 151–154 (2013).
[45]D. J. Hoffman, H. A. Bechtel, D. A. Huyke, J. G. Santiago, D. P. DePonte, and J. D. Koralek, Langmuir **38**, 12822–12832 (2022).
[46]M. Faubel and B. Steiner, Ber. Bunsenges. Phys. Chem. **96**, 1167–1172 (1992).
[47]J. Nishitani, S. Karashima, C. W. West, and T. Suzuki, J. Chem. Phys. **152**, 144503 (2020).
[48]M. N. Pohl, E. Muchová, R. Seidel, H. Ali, Š. Sršeň, I. Wilkinson, B. Winter, and P. Slavíček, Chem. Sci. **10**, 848–865 (2019).
[49]B. Winter, R. Weber, P. M. Schmidt, I. V. Hertel, M. Faubel, L. Vrbka, and P. Jungwirth, J. Phys. Chem. B **108**, 14558–14564 (2004).
[50]N. Ottosson, M. Faubel, S. E. Bradforth, P. Jungwirth, and B. Winter, J. Electron Spectrosc. Relat. Phenom. **177**, 60–70 (2010).
[51]T. Buttersack, H. Haak, H. Bluhm, U. Hergenhahn, G. Meijer, and B. Winter, "Imaging temperature and thickness of thin planar liquid water jets in vacuum," arXiv:2304.02967 [cond-mat] (2023).
[52]S. Koneshan, J. C. Rasaiah, R. M. Lynden-Bell, and S. H. Lee, J. Phys. Chem. B **102**, 4193–4204 (1998).
[53]Y.-P. Chang, Z. Yin, T. Balciunas, H. J. Wörner, and J.-P. Wolf, Struct. Dyn. **9**, 014901 (2022).
[54]H. Siegbahn and M. Lundholm, J. Electron Spectrosc. Relat. Phenom. **28**, 135–138 (1982).
[55]A. Vegiri, J. Mol. Liq. **112**, 107–116 (2004).
[56]H. Elgabarty, N. K. Kaliannan, and T. D. Kühne, Sci. Rep. **9**, 10002 (2019).
[57]J. T. Russell, Y. Lin, A. Böker, L. Su, P. Carl, H. Zettl, J. He, K. Sill, R. Tangirala, T. Emrick, K. Littrell, P. Thiyagarajan, D. Cookson, A. Fery, Q. Wang, and T. P. Russell, Angew. Chem., Int. Ed. **44**, 2420–2426 (2005).
[58]G. Luo, S. Malkova, J. Yoon, D. G. Schultz, B. Lin, M. Meron, I. Benjamin, P. Vanýsek, and M. L. Schlossman, Science **311**, 216–218 (2006).
[59]K. Piradashvili, E. M. Alexandrino, F. R. Wurm, and K. Landfester, Chem. Rev. **116**, 2141–2169 (2016).
[60]L. Lin, A. U. Chowdhury, Y.-Z. Ma, R. L. Sacci, J. Katsaras, K. Hong, C. P. Collier, J.-M. Y. Carrillo, and B. Doughty, J. Phys. Chem. B **126**, 2316–2323 (2022).
[61]R. J. Phipps, G. L. Hamilton, and F. D. Toste, Nat. Chem. **4**, 603–614 (2012).
[62]M. L. Schlossman, Curr. Opin. Colloid Interface Sci. **7**, 235–243 (2002).